# Cavity Ring-Down Spectroscopy Sensor for Real Time In Situ Measurement of Sputter Erosion in Anode Layer Type Hall Thrusters

**IEPC-2009-147**

*Presented at the 31st International Electric Propulsion Conference,*
*University of Michigan • Ann Arbor, Michigan • USA*
*September 20 – 24, 2009*

Naoji Yamamoto[1]
*Kyushu University, Kasuga, Fukuoka, 816-8580, Japan*

Lei Tao[2], Binyamin Rubin[3], John D. Williams[4] and Azer P.Yalin[5]
*Colorado State University, Fort Collins, CO, 80523, USA*

**Abstract: A Sputter monitoring system using continuous-wave cavity ring-down spectroscopy (cw-CRDS) was built for both lifetime assessment and contamination effects in Hall thrusters. First, we have performed proof of measurements of sputtered manganese atoms from manganese-iron alloy plate. The measurement strategy is based upon detection of manganese atoms via an absorption line from ground state at a wavelength of 403.076 nm. The hyperfine structure of the manganese spectrum can be observed owing to honeycomb structure mount as a velocity-filter. The number density estimated by CRDS is reasonable as comparison with simple estimates. These results validate the estimation of the erosion rate by CRDS. Next, we apply this system for erosion atoms from the acceleration channel wall (stainless steel 316) in an anode layer type Hall thruster. The path-integrated number density is $8.2 \pm 1.5 \times 10^{12}$ m$^{-2}$ at discharge voltage of 150 V and argon mass flow rate of 70 sccm. The number density is proportional to the discharge voltage, as expected. The number density and mass-loss have a relatively linear dependence. These results show the validity of the erosion sensor for Hall thruster lifetime estimation.**

## Nomenclature

| | | |
|---|---|---|
| $Aki$ | = | Einstein $A$ coefficient, 1/s |
| $Abs$ | = | Absorbance |
| $c$ | = | Speed of light, 2.998 x $10^8$ m/s |
| $E_b$ | = | Binding energy, J |
| $E_i$ | = | Energy of state $i$, J |
| $E_k$ | = | Energy of state $k$, J |
| $g_i$ | = | Degeneracy of state $i$ |
| $g_k$ | = | Degeneracy of state $k$ |
| $k(\nu)$ | = | Absorption coefficient, m$^{-1}$ |
| $l$ | = | Length of the ring-down cavity, m |

[1] Assistant Professor, Department of Advanced Energy Engineering Science, yamamoto@aees.kyushu-u.ac.jp
[2] Doctoral candidate, Department of Mechanical Engineering, leitao@lamar.acns.colostate.edu.
[3] Post-Doctoral Researcher, Department of Mechanical Engineering, brubin@engr.colostate.edu.
[4] Associate Professor, Department of Mechanical Engineering, john.d.williams@colostate.edu.
[5] Associate Professor, Department of Mechanical Engineering, azer.yalin@colostate.edu.

| | | |
|---|---|---|
| $Ni$ | = | Lower state concentration, $m^{-3}$ |
| $R$ | = | Mirror reflectivity |
| $S(t,\nu)$ | = | Ring-down signal |
| $x$ | = | Position along the optical axis |
| $\nu$ | = | Laser frequency, Hz |
| $\tau$ | = | Ring-down time, s |
| $\tau 0$ | = | Empty cavity ring-down time, s |

## I. Introduction

Hall thrusters are a class of electric propulsion device in which a propellant gas is ionized and accelerated to produce thrust. [1-3] They offer an attractive combination of high thrust efficiency (exceeding 50%) and specific impulse (~1500-3000 sec). In comparison to chemical rockets, the high specific impulse is attractive for large delta V missions such as satellite positioning and station-keeping, and space exploration. Hall thrusters also have a higher thrust density than ion thrusters due to the existence of electrons in the ion acceleration zone. In addition, the lack of grids is attractive owing to the potential for reduced failures. Since the 1970s over 200 Hall thrusters have been operated in space. A key requirement for the practical use of Hall thrusters is the ability to operate for long durations, for example a Hall thruster used for north-south station keeping (NSSK) of a commercial spacecraft will have to operate for over 5,000 hours over the course of its mission.[4,5] The primary life-limiter for Hall thrusters is acceleration channel wall erosion.[6,7] A thruster is generally considered to have reached end of life when the channel is fully eroded and the underlying magnetic yoke becomes exposed. The physical mechanism causing the erosion is sputtering of the channel material due to bombardment by energetic particles, primarily propellant ions having undergone radial acceleration. In addition to causing channel erosion and associated lifetime concerns, sputtered particles can redeposit on spacecraft components such as solar-arrays, thereby degrading their performance and potentially compromising spacecraft operation

There have been many studies on the lifetime of Hall thrusters, including endurance tests,[4,5] numerical modeling.[8,9] and direct measurement of erosion materials. These studies show that the erosion depends on operating condition, magnetic field configuration, wall material, anode configuration, and channel geometry. Understanding this dependence is essential for the practical application of Hall thrusters. It is not, however, practicable to validate the lifetime at each condition by means of typical wear tests because of the huge costs in time and money: several hundred thousand to millions of dollars and tie up valuable vacuum facilities and engineers for several months. What is needed, therefore, is a method of measuring thruster erosion rates non-intrusively in real- or near-real-time. The erosion rate can be measured by probing the eroded wall material in the plume. Such measurements would allow simultaneous evaluation of the impact of Hall thruster design changes on performance and lifetime.

The ideal diagnostic for *in situ* thruster studies should have high sensitivity to measure low erosion rates, the possibility of integration to a thruster test-facility, and fast time-response to explore a range of operating conditions. Techniques such as weight loss,[10] collector plate,[11] quartz crystal microbalance,[12,13] radioactive tracers,[14] mass spectrometry,[15] and Rutherford backscattering[16] each have certain advantages and can be appropriate for material sputter characterization studies but none readily meets all of the above criteria. The need for a sensitive nonintrusive measurement suggests the use of optical techniques. Optical emission spectroscopy (OES),[17,18] laser induced fluorescence (LIF) [19] and multi-photon ionization coupled to a time of flight mass spectrometer[20,21] have been used for species-specific sputtering measurements. The use of LIF has been particularly extensive and has proven to be very effective for velocity measurement though challenging for quantitative number density. OES is attractive owing to its experimental simplicity but the analysis can be challenging since collisional-radiative modeling (or similar) is required to extract number densities. Owing to these limitations, Laser Absorption Spectroscopy (LAS) has been proposed for erosion rate measurement[9]. LAS is a non-intrusive optical method with the potential advantage of providing directly quantitative number density measurements (meaning it does not require external calibration). Furthermore, LAS is amenable to *in situ* studies which can be conducted in near real-time. Our previous research showed the possibility of nonintrusive near real-time erosion measurement by LAS in an anode layer type Hall thruster[9]; however, the approach didn't yield sufficient sensitivity for number density measurements at needed conditions. The approach presented here builds upon our previous development of cavity ring-down spectroscopy (CRDS)[22-24] for sputtering measurements. CRDS is a path-enhanced laser absorption method that provides the ultra-high sensitivity required to measure low erosion rates. Our current focus is to develop a CRDS lifetime sensor for Hall thruster erosion studies.

Past work at Colorado State University (CSU) has shown the use of pulsed-CRDS/continuous wave-CRDS to quantitatively measure sputter products.[25-29] We view that CRDS can function both as a method for sputter yield measurement and material characterization, to generate inputs for erosion and lifetime modeling; and can also provide an *in situ* diagnostic suitable to study thruster erosion and lifetime and aid in thruster design. Development on an *in situ* sputter sensor is underway in a collaborative effort between researchers at CSU, University of Michigan (UM), and Kyushu University (KU).

The layout of the remainder of the paper is as follows. Section II of the paper describes the demonstration of the manganese cw-CRDS sensor. Section III presents the experimental setup and results used for the erosion sensor of the anode layer type Hall thruster. For this class of thruster the acceleration channel is generally formed from a conductive material. Our proof of principle experiments employed a stainless steel channel and erosion was measured by probing the sputtered manganese atoms (contained within the stainless steel). For optimum sensitivity we have implemented CRDS with a continuous-wave (cw) laser as opposed to a pulsed laser source. The sensor was used to measure the path-integrated concentration of sputtered manganese at different thruster operating conditions. The CRDS results are validated against mass-loss measurements. Relating the CRDS number density measurements to the mass-loss requires consideration of the flux of the sputtered particles, for which we have used as simple finite element model. Finally, conclusions are presented in Section IV.

## II. Manganese CRDS sensor

We have performed proof of sensitivity and time response of the sputtered material sensor using cw- CRDS in a diagnostic chamber. The target is manganese from a Mn-Fe alloy. We use a tunable diode laser with external cavity (ECLD) to measure the transition line of manganese at 403.076 nm (Air). The transition data for this measurement, $E_i$, $E_k$, $A_{ki}$, $g_i$, $g_k$ are 0, 3.075, $1.7\times10^7$, 6, 8, respectively, as quoted from the NIST database[30]. The modehop free tuning range of the laser is about 30 GHz and the laser linewidth is less than 5 MHz. An optical isolator and Single Mode FC/APC fiber are used to prevent back reflections into the laser. An aspheric lens is used at the fiber exit to collimate the beam and to match the beam to $TEM_{00}$ mode of the cavity. A threshold detection circuit and an acousto-optic modulator (AOM) are used to extinguish the incoming laser beam, as shown in Fig.1. The combined time response of the threshold circuit and AOM firing is less than 400 ns. A photomultiplier tube is used as a detector and positioned behind the cavity. A dielectric interference filter and an iris are used to suppress background light and the emission from the plasma. Ring-down signals are measured with a 20 MHz 12-bit analog-to-digital acquisition board connected to a personal computer, and a custom Labview program is used for exponential fitting with the nonlinear Levenberg–Marquardt fit. A solid etalon (free spectral range=2.26 GHz) is used as a frequency reference. The optical cavity length is 0.83 m and is formed by a pair of high reflectivity mirrors (Los Gatos Research, R>99.995), each 25.4 mm in diameter with radius-of-curvature of 1 m. We typically operate with empty-cavity ring-down times of ~20$\mu$s, corresponding to R~99.986% (close to manufacturer's specifications). The mirrors are held in custom mounts affixed to the end of extender arms connected to the vacuum chamber. The mounts are mechanically and thermally isolated from the main chamber body by using bellows in line with the arms. A series of irises (diameter ~ 5 mm) are set to the arms in order to prevent the mirrors from deposition of sputtered particles. With this method, minimal degradation of mirror reflectivity has been observed (~5-10 ppm/hour). Improved shielding and/or periodic cleaning would be required for longer term operation.

For demonstrating the real-time monitoring of the sputtered material, sputtered manganese from a Mn-Fe alloy target(8 cm × 4 cm, 50% manganese and 50% iron by mole ratio) was detected. The ion beam is extracted from an 8-cm diameter structurally integrated thruster obtained from NASA, and modified to operate on an inert gas, and to use thoriated tungsten filaments for both the main and neutralizer cathodes in place of the hollow cathodes used in the original design. The ion beam current and voltage were 120 mA and 750 V respectively. We have used a honeycomb structure mounted on the target to accentuate the hyperfine structure of the spectrum[31]. The axis of the honeycomb cells (3 cm high) is aligned normally to the target surface so that the incident ion beam is minimally affected en route to the target. The side-walls of the honeycomb act as a velocity-filter: Particles leaving

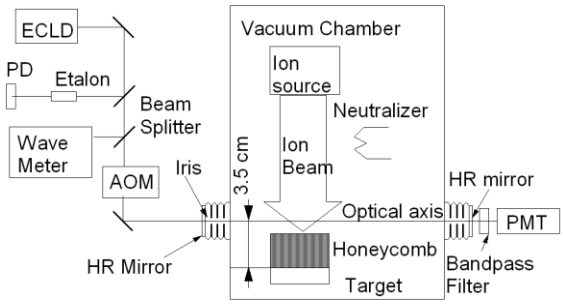


**Figure 1. Schematic diagram of real-time monitoring system.**

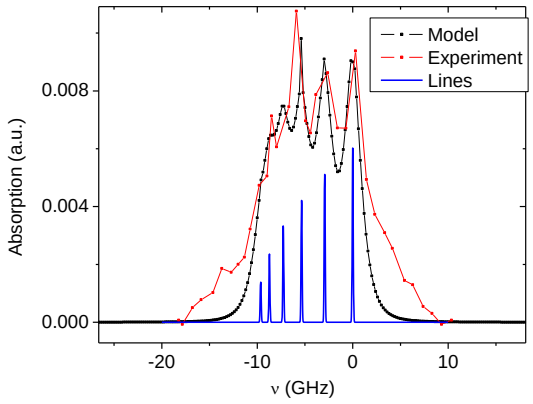


**Figure 2. Absorption spectrum of manganese with a theoretical simulation.**

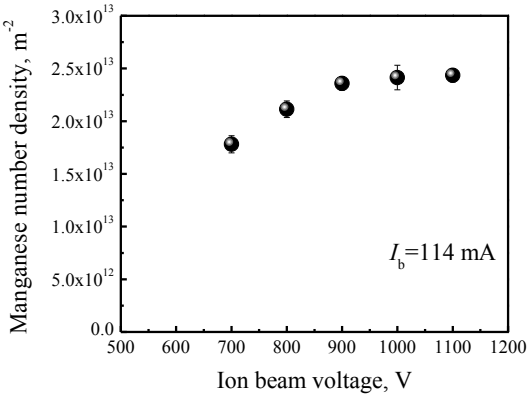


**Figure 3. The relation between path-integrated manganese number density and ion beam voltage.**

the target surface approximately normally escape, while particles leaving the surface at angles of greater than ~20 degrees from the surface normal are deposited on the side-walls of the honeycomb. The result is that the particles in the CRDS measurement region are more orthogonal to the optical-axis and have smaller Doppler shift contributions so that the form of the hyperfine spectrum is better preserved (less broadened).

Figure 2 shows an absorption profile of target spectrum. Again, a modeled spectrum is computed and shown in the figure. The model (described above) uses hyperfine shifts and relative strengths reported in the literature. To incorporate the geometry of the honeycomb we assume that particles sputtered with angles larger than 20 degrees from the surface normal make no contribution to the signal. The laser lineshape is not included in the model owing to its small width (~5 MHz) relative to the measured and modeled features. We can see relatively good agreement between modeled and measured spectrum. The wider wings of the lineshape in the data relative to the model are primarily owing to a background manganese signal caused by the outer portions of the ion beam hitting the stainless steel chamber wall. We have verified this background signal exists by masking our target in which case we still measure a weak manganese absorption feature of an amplitude consistent with providing the aforementioned wings.

Figure 3 shows the relation between path-integrated manganese number density and ion beam voltage at beam current of 114 mA. The manganese number density increase with the ion beam voltage and the value of the number density is reasonable as comparison with simple estimates based on the ion beam current profile, target dimension, and tabulated sputter yields. These results showed the CRDS measurements give us not only information about the concentration of the sputtered atoms but also the velocity distribution.

## III. Erosion sensor of the anode layer type Hall thruster

### A. Experimental Setup

Figure 4 shows a diagram of the experimental setup emphasizing the CRDS aspects. The laser is coupled to a polarization maintaining (PM) single mode FC/APC fiber, which goes though the feedthrough into the vacuum

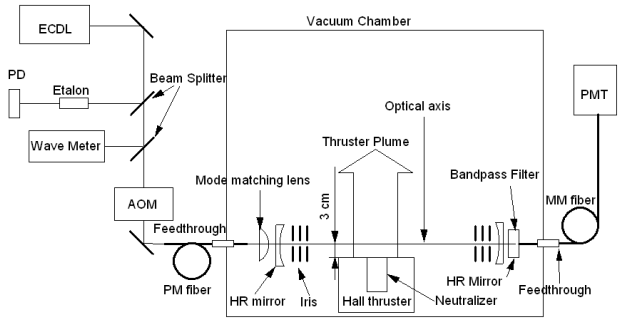


**Figure 4. Schematic diagram of Mn monitoring system**

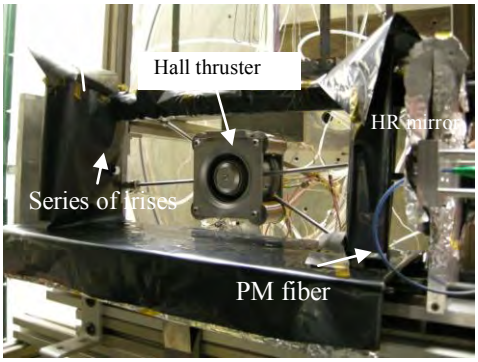


**Figure 5. Picture of optical cavity hardware on a rail-system Manganese Rail system.**

chamber. An aspheric lens is used at the fiber exit to collimate the beam and to match the beam to $TEM_{00}$ mode of the cavity. The optical cavity length is 0.70 m and is formed by a pair of high reflectivity (HR) mirrors (Los Gatos Research, R>99.995%), each 25.4 mm in diameter with radius-of-curvature of 1 m.

The optical cavity hardware is on a rail-system inside of the chamber, as shown in Fig.5. The rail system is mechanically and thermally isolated from the main chamber body by using polyurethane bumpers. The optical axis is 3 cm downstream of the thruster and it goes through the axis of the thruster. A series of irises held within a re-entrant tube are positioned in front of each cavity mirror to prevent deposition of sputtered particles and excess exposure to ultraviolet light, both of which can degrade mirror reflectivity. Light exiting the cavity is relayed via a multi-mode (MM) optical fiber to a PMT outside the vacuum chamber. A dielectric interference filter (40 nm band-pass) and an iris are used to suppress background light and emission from the plasma.

Figure 6 shows a cross-section of the 1 kW class anode layer type Hall thruster used in the current experiments. The inner and outer diameters of the acceleration channel are 48 mm and 72 mm respectively. An inner solenoid coil and four outer solenoid coils create a predominantly radial magnetic field in the acceleration channel, as shown in Fig. 7. The magnetic flux density is varied by changing the coil current. The magnetic field distribution along the channel median is shown in Fig. 7(a) and the calculated magnetic field lines is shown in Fig. 7(b) (each coil current is 1 A, calculated using Magnum2.5, Field Precision LLC.). The origin of Fig.7 is the exit of the acceleration channel, and the radial magnetic flux density has peak at $z$ = -1 mm. In these experiments, the acceleration channel is made from stainless steel (SUS316). The SUS 316 contains about 1% manganese (0.81% from manufacturer's datasheet) and, as discussed below, the CRDS measurements are based on detection of the manganese sputtered from the channel wall. The separation between the acceleration channel wall and the anode is 1 mm. The thruster has a hollow annular anode, which consists of two cylindrical rings, with a propellant gas fed through them. The width of the hollow anode is 8 mm, and the gap between the tip of the anode and the exit of the acceleration channel is fixed at 3 mm. High-purity (99.999%) argon gas was used as the propellant with thermal mass flow controllers (Brooks 5850E).

Tests are conducted in a vacuum chamber of 1.5 m diameter by 4.6 m length. A hollow cathode is used as the electron source. The pumping system includes a dry mechanical pump (Edwards GV250), assisted by a mechanical booster pump (Edwards EH-1200) and two

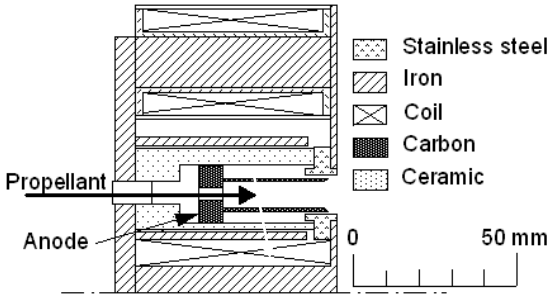


**Figure 6. Cross section of the Anode layer type Hall thruster developed at Kyushu University.**

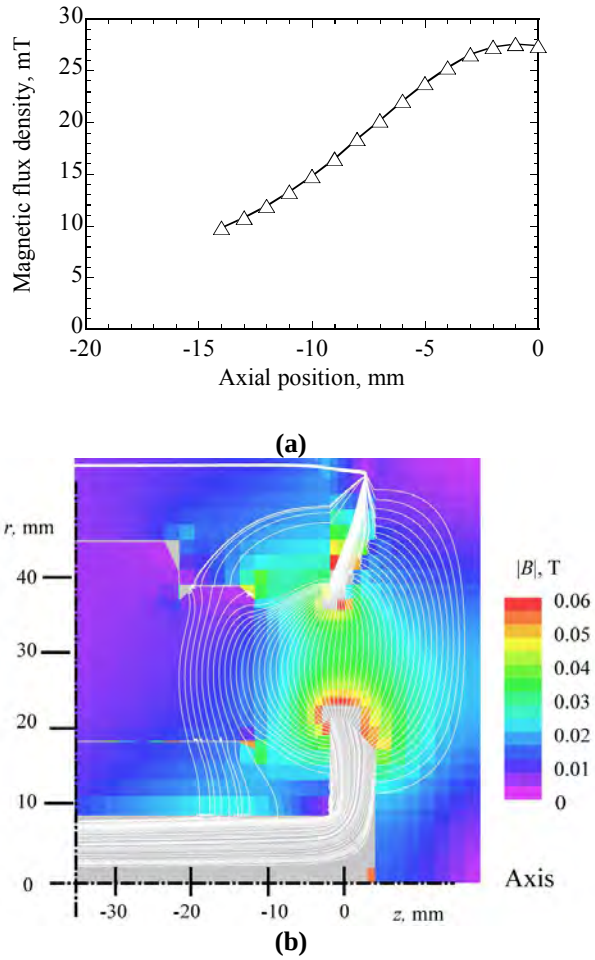


**Figure 7. Magnetic field configuration of the Hall thruster developed at Kyushu University. (a) Radial magnetic flux density profile (outer coil current = 1 A, inner coil current= 1A, *r*=30 mm) (b) Calculated magnetic field lines (Calculated using calculated using Magnum2.5, Field Precision LLC.)**

diffusion pumps (Varian HS-20). The chamber baseline pressure is below $7x10^{-4}$ Pa. Any contribution of sputtered manganese from the chamber wall is negligible owing to the chamber wall material (soft iron) and position of the Hall thruster.

**B. Results of the erosion sensor for anode layer type Hall thruster**

Concentration measurements are determined from the area of absorption spectra, as shown in Fig. 8. To construct the spectrum, we use a binning approach, dividing the frequency axis into a series of bins, each with width 1 GHz, and signals falling within the bin are averaged. The path-integrated manganese number density is estimated using equation (3). The laser tuning range is insufficient to scan over the full line width so we find the line area by numerically integrating half of the lineshape (the low-frequency side of the peak) and doubling. In future work other scanning and fitting methods could be used. For the condition that discharge voltage = 150 V and argon anode mass flow rate = 70 sccm, the path-integrated Mn concentration is $8.2 \pm 1.5 \times 10^{12}$ $m^{-2}$ (where the uncertainty is partly due to the area fitting but dominated by the 18% uncertainty in $A_{ki}$). In principle the measured concentration corresponds to the directly measured ground state, but because there are no low-lying levels the ground state and overall Mn populations are equivalent (to within our uncertainty). More precisely, a Boltzmann analysis for a characteristic temperature of 1500 K shows that the ground state comprises >99% of the overall population. It is interesting to note that owing to lack of equilibrium in the sputtering process (and lack of collisions after ejection) there is little reason to assume Boltzmann distributions for the sputtered particles; nonetheless, past research has generally shown distributions similar to Boltzmann with "temperatures" generally in the range ~500-1500 K. (In some cases elevated "anomalous" populations of sputtered particles in higher lying energy levels have been observed, but the agreement between our CRDS and mass-loss makes it unlikely that such effects are significant in these experiments.) One should also consider the possibility that sputtered ground state atoms are excited to a higher level, or ionized, prior to reaching the measurement location, but simple calculations show the loss of ground state atoms owing to these effects to change the signal by <10% at our conditions.

For quantitative validation of the CRDS measurement, we have performed mass-loss tests of one-hour duration. Figure 9 shows estimated mass loss determined from the CRDS measurements and mass-loss of one-hour duration for three different discharge voltages. Erosion rate deduced from the CRDS are quantitatively in good agreement with the direct mass-loss measurements. The mass-loss values are found by measuring the mass change of the stainless steel channel at the corresponding condition (with uncertainty of 5% due to scale resolution and small changes in thruster operation conditions). For the estimation of mass loss deduced from the CRDS results, we use a finite element model for the sputtering.[26] We consider sputtering from the edge of the acceleration channel walls (from 3mm upstream of the channel exit). Identification of these surfaces is based on visual inspection of the channel. We assume that particles are ejected with a diffuse sputter yield distribution, i.e. proportional to the cosine of the ejection angle relative to the surface normal, and we assume a Thomson distribution for particle velocity (energy) using the binding energy of Mn ($E_b$ = 2.92 eV) and $n$=1.54 as the exponent on the velocity distribution. [26] We make a series of elements on each sputtering surface and along the optical beam, and then find sputter contributions from each source location to each location along the optical axis. These contributions are added together to determine the path-integrated number density. We determine the corresponding expected mass-loss from

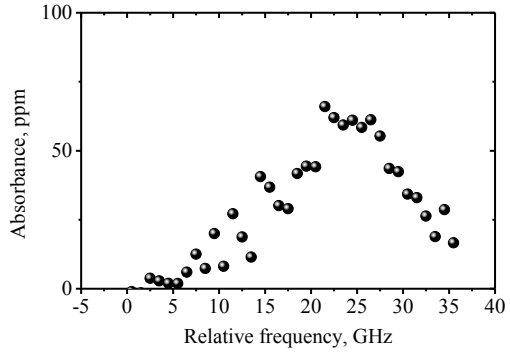


**Figure 7. Absorption profile of target spectrum at discharge voltage of 150 V and argon anode mass flow rate of 70 sccm.**

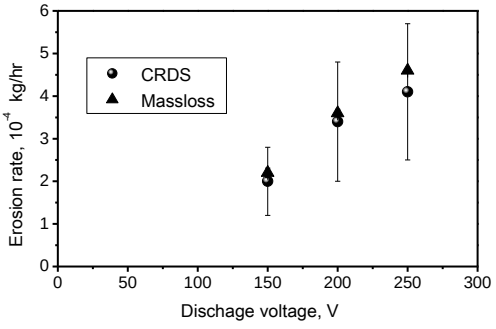


**Figure 8. Mass erosion rates from found direct mass loss measurement and estimated from the CRDS sensor.**

the flux of particles (neglecting re-deposition). We assume that the composition of species sputtered from the steel mimics the composition of the bulk steel in order to find the total mass flux (of all species). In this way we can find the proportionality factor between the Mn number density along the optical axis (i.e. the CRDS measurement) and the associated total mass flux (mass erosion rate), and use this factor to determine mass erosion rates from the CRDS measurements. The uncertainty in the (CRDS) modeled erosion values (± 40%) are found from contributions due to possible variation of the sputter flux from each surface (we consider cases where each surface sputters at a rate of twice the others (± 16%)), changes from diffuse sputter yield to an over- or under-cosine profile (± 5%), changing the exponent used in the Thomson distribution (± 32%), and the uncertainty in corresponding CRDS number density measurement (± 18%). The overall uncertainty in CRDS erosion rate is rather high but could be improved in several ways including more accurate determination of the $A_{ki}$ coefficient, spatial scanning with Abel inversion to lower the geometric contribution to the uncertainty, and better knowledge of the velocity distribution (e.g. by CRDS lineshape studies or complementary LIF measurements). The model also allows simulation of the absorption lineshape based on Doppler shifts.[26, 28] A modeled lineshape computed with the above assumptions and including the hyperfine structure of manganese is in reasonable agreement with the measured lineshape.

For these conditions, the erosion rate increases roughly linearly with discharge voltage. This is reasonable since a sputtering yield increases with the argon ion energy colliding with wall, and argon ion energy increases with the discharge voltage.

## IV. Conclusion

The cw-CRDS real-time sputter monitoring system reported here is, to the best of our knowledge, the first such demonstration. The demonstrated cw-CRDS sensor used a diode laser at 403 nm to probe manganese atoms sputtered from the stainless steel acceleration channel of a 1 kW class anode layer Hall thruster. The optical cavity was fiber coupled in and out of the vacuum chamber. The flexibility of such an approach is amenable to implementation in different vacuum chamber facilities. We have compared the erosion rate estimated from the cw-CRDS technique and the mass-loss of one-hour duration for three different discharge voltages. The good agreement between the directly measured mass erosion rate and that determined from the CRDS, and between the measured and modeled CRDS lineshape, shows the validity of the CRDS erosion sensor. Furthermore, the high time response and /in situ/ nature of the CRDS sensor can be of great utility in understanding erosion rate trends, i.e. monitoring how the erosion signal varies with changes in thruster operating conditions. The aforementioned results showed that cw-CRDS based sensors should allow (near) real time measurements of sputter erosion in Hall thrusters, thereby providing a new and powerful tool for sputter erosion and lifetime studies. Indeed, we are currently developing a similar erosion sensor for magnetic layer type Hall thrusters. This sensor employs cw-CRDS with a frequency-quadrupled diode laser to detect sputtered boron from the boron nitride insulator channel. Initial tests show a minimum detectable absorbance of 20 ppm for detection times of ~1 minute which should be very adequate for many thruster conditions[34)].

## Acknowledgments

The authors thank Prof. Alec Gallimore for collaboration in this enterprise and thank the Japan Society for the Promotion of Science, Japan for their financial support through a Grant-in-Aid for Scientific Research (S), No. 16106012.

## References

[1] Kaufman, H. R., "Technology of Closed-Drift Thrusters," *AIAA Journal*, Vol. **23**, No. 1, (1985) pp. 78–86.

[2] Kim, V., "Main physical features and processes determining the performance of stationary plasma thrusters," *Journal of Propulsion and Power*, Vol. **14**, No. 5, (1998) pp. 736–743.

[3] Choueiri, E. Y., "Fundamental difference between the two Hall Thruster Variants," *Physics of Plasmas*, Vol. **8**, No. 11, (2001) pp. 5025–5033.

[4] Garner, C. E., Polk, J. E., Goodfellow, K. D., and Brophy, J. R.: Performance Evaluation and Life Testing of the SPT-100, IEPC paper 93-091, Sept. 1993.

[5] Garner, C. E., Brophy, J. R., Polk, J. E., and Pless, L. C.: A 5730-Hr Cyclic Endurance Test of the SPT-100, AIAA paper 95-2667, July 1995.

[6] Jacobson , D. and Manzella, D., "High Voltage TAL Erosion Characterization," AIAA paper 2002-4257 July, 2002.

[7] Yamamoto, N., Yokota, S., Matsui, M., Komurasaki, K., Arakawa, Y.: Measurement of Erosion Rate by Absorption Spectroscopy in a Hall Thruster, *Review of Scientific Instruments*, **76**, Issue 8, (2005) 083111.

[8] Shannon Y. Cheng and Martinez-Sanchez, M., "Hybrid Particle-in-Cell Erosion Modeling of Two Hall Thrusters," *Journal of Propulsion and Power*, Vol. **24**, No. 5 (2008) pp. 987-998.
[9] Eagle, W. E,. , Boyd,I. D., Trepp, S. G., Sedwick, R. J., "The Erosion Prediction Impact on Current Hall Thruster Model Development," AIAA paper -2008-5087, July, 2008.
[10] Yalin, A. P., Surla, V., Farnell, C., Butweiller, M., and Williams, J. D.: Sputtering studies of multi-component materials by weight loss and cavity ring-down spectroscopy, AIAA paper 2006-4338, July, 2006.
[11] Tsuge, H. and Esho, S.: Angular distribution of sputtered atoms from polycrystalline metal targets, *J. Appl. Phys.* **52** (1981) pp.4391-4395.
[12] Yalin, A. P., Williams, J. D., Surla, V. and Zoerb, K. A.: Differential Sputter Yield Profiles of Molybdenum due to Bombardment by Low Energy Xenon Ions at Normal and Oblique Incidence, *J. Phys. D: Appl. Phys.* **40** (2007) pp. 3194–3202.
[13] Mannami, M., Kimura, K., and Kyoshima, A.: Angular distribution measurements of sputtered Au atoms with quartz oscillator microbalances, *Nuclear Instruments and Methods,* **185** (1981) pp.533-537
[14] Kundu, S., Ghose, D., Basu, D., and Karmohapatro, S. B.: The angular distribution of sputtered silver atoms, *Nuclear Instruments and Methods in Physics Research B* **12** (1985) pp.352-357.
[15] Wucher, A. and Reuter, W.: Angular distribution of sputtered particles from metals and alloys, *J. Vac. Sci. Tech. A* **6,** 4 (1988) pp.2316-2318.
[16] Mantenieks, M., Foster, J., Ray P., Shutthanandan, S., and Thevuthasan, T.: Low energy xenon ion sputtering yield measurements, IEPC paper 01-309, 2001
[17] Andersen, N., B. Andresen, and Veje, E.: Atomic excitations in sputtering processes, *Radiation Effects,* **60** (1982) pp.119-127.
[18] Doerner, R.P., Whyte, D.G., and Goebel, D.M.: Sputtering yield measurements during low energy xenon plasma bombardment, *J. App. Phys.* **93**(9) (2003) pp.5816-5823.
[19] Pellin, M.J., Wright, R.B., and Gruen, D.M.: Laser fluorescence spectroscopy of sputtered zirconium atoms, *J. Chem. Phys.* **74** (1981) pp.6448-6457
[20] Nicolussi, G., *et al*.: Formation of metastable excited Ti and Ni atoms during sputtering, *Phys. Rev. B* **51**, 14 (1995) pp.8779-8788.
[21] Goehlich, A.: Investigation of time-of-flight and energy distributions of atoms and molecules sputtered from oxygen-covered metal surfaces by laser techniques, *Appl. Phys. A*. **72** (2001) pp.523-529.
[22] Busch K. W. and Busch M.A. :Cavity-Ringdown Spectroscopy, American Chemical Society, Washington DC,(1999) pp.7-19.
[23] Zalicki, P. and Zare, R.N.: Cavity ring-down spectroscopy for quantitative absorption measurements, *J. of Chemical Physics*, **102**, 7 (1995) pp. 2708-2717.
[24] Yalin, A.P., and Zare, R.N.: Effect of Laser Lineshape on the Quantitative Analysis of Cavity Ring-Down Signals, *Laser Physics*, **12**, 8, (2002) pp. 1065-1072.
[25] Surla,V. Wilbur, P.J. Williams, J.D. Johnson,M. Yalin, A.P.: Sputter Erosion Measurements of Titanium and Molybdenum by Cavity Ring-Down Spectroscopy, *Review of Scientific Instruments*, **75**, 9, (2004) pp. 3025-3030.
[26] Yalin, A.P., Surla, V., Butweiller, M., Williams, J.D.: Detection of Sputtered Metals using Cavity Ring-Down Spectroscopy, *Applied Optics*, **44**, 30 (2005) pp. 6496-6505.
[27] Yalin, A.P., Surla, V.: Determination of Number Density and Velocity of Sputtered Particles by Cavity Ring-Down Spectroscopy, IEPC paper 2005-300, Oct. 2005.
[28] Yalin, A.P., Surla, V.: Velocity Measurements by Cavity Ring-Down Spectroscopy, *Optics Letters*, **30**, (2005) pp. 3219-3221
[29] Tao, L., Yamamoto, N. and Yalin, A.P.: Cavity Ring-Down Spectroscopy Sensor for Ion Beam Etch Monitoring and End-Point Detection of Multilayer Structures, *Review of Scientific Instruments* **79** (2008) 115107.
[30] http://www.physics.nist.gov/cgi-bin/ASD/lines1.pl
[31] Booth, A. J., Shallis, M. J. and Wells, M., : Hyperfine structure measurements for lines of astrophysical interest in MN I,Royal Astronomical Society, Monthly Notices (ISSN 0035-8711), Vol. 205, Oct. (1983), p. 191-205.
[32] Surla, V. and Yalin, A. P.: Differential sputter yield measurements using cavity ring-down spectroscopy, Applied Optics, Vol. 46, Issue 19 (2007) pp. 3987-3994.